Available online at www.sciencedirect.com
SCIENCE DIRECT®
ELSEVIER
International Journal of Solids and Structures 43 (2006) 1490–1504
INTERNATIONAL JOURNAL OF SOLIDS and STRUCTURES
www.elsevier.com/locate/ijsolstr

Elastodynamic analysis of low tension cables using a new curved beam element

Z.H. Zhu, S.A. Meguid *

Department of Mechanical and Industrial Engineering, Engineering Mechanics and Design Laboratory, University of Toronto, 5 King's College Road, Toronto, Ontario, Canada M5S 7G8

Received 18 November 2004; received in revised form 16 March 2005
Available online 21 April 2005

Abstract

In this paper, we address and overcome the difficulties associated with the use of the classic cable theory to treat low tension cables by developing a new three-noded locking-free nonlinear curved beam element. Based upon nonlinear generalized curved beam theory, large deformations and rotations in the new element are formulated in terms of Updated Lagrangian framework. Consistently coupled polynomial displacement fields are used to satisfy the membrane locking-free condition and the requirement of being able to recover the inextensible bending modes. Quintic transverse displacement interpolation functions are used to represent the bending deformation of the beam, while the axial and torsional displacement fields are derived by integration of the presumably linear membrane and torsional shear strain fields, which are coupled with the transverse displacement fields. Numerical results are presented to demonstrate the superior accuracy and the high convergence rate of the newly developed curved beam element. The stability and accuracy of the new element are further validated by experiments of an instrumented free-swinging steel cable experiencing slack and low tension. Good agreements in cable position and tension are observed between the experimental results and the finite element predictions.

Keywords: Curved beam element; Curvilinear strain; Membrane locking; Low tension cable; Cable dynamics; Nonlinear finite element; Updated Lagrange framework

* Corresponding author. Present Address: Aerospace Engineering Division, MAE, Nanyang Technological University, Singapore. Tel.: +1 416 978 5741; fax: +1 416 978 7753.
E-mail address: meguid@mie.utoronto.ca (S.A. Meguid).

0020-7683/$ - see front matter © 2005 Elsevier Ltd. All rights reserved.
doi:10.1016/j.ijsolstr.2005.03.053

1. Introduction

Cables have widely been used in industry as an economic mean to transmit forces and carry payloads over great distances. However, a low working tension in the cables such as that experienced in aerial tow cable (Leonard and Recker, 1972), aerial refueling hose (Vassberg et al., 2002), cable towed sonar and remote operated vehicles in deep sea (Vassalos and Huang, 1996; Sun and Leonard, 1998) may result in unstable behaviors resulting from cable slacking (Wu et al., 2003). The unstable behavior of low tension cables under dynamic loading could cause excessive tension spikes in the cable leading to catastrophic failures, such as premature cable breakage (Phillips, 1949).

Many studies have been carried out for the analysis of low tension cable problems using the classic cable theory and the finite difference method. The classic cable theory simplifies the cable as a tensile member that cannot resist compressive, bending and torsional loads. However, unlike high tension cable problems, the basic mechanism of energy propagation in low tension cables is changed from membrane dominant state to bending dominant state when the cable tension disappears (Burgess, 1992). The classic cable theory becomes singular when the tension disappears in any part of the cable (Howell, 1992). The limitations of the existing approaches create a need for alternative approaches to treat the low tension cable problems. Many works (Buckham and Nahon, 1999; Howell, 1992; Burgess, 1992; Koh et al., 1999; Wu et al., 2003) have been carried out to alleviate the low tension cable problems by adding artificial damping, higher order terms and bending stiffness of cable. Among them, only the approach based on the beam theory is a natural extension of the classic cable theory and has a sound theoretical foundation and physical meaning.

The modeling of the low tension cables with a realistic and robust description of cable dynamics inevitably leads to a complex mathematical problem and consequently requires numerical solution techniques, such as, lumped parameter (Buckham and Nahon, 1999), finite segment (Delmer et al., 1988), finite difference (Koh et al., 1999), and finite element (Zhu et al., 2001; Rizzo, 1991). Among all the numerical methods, the finite element method is probably the most appealing technique. The main advantage of the finite element method over other methods is its capability to handle complex geometries with multiple cable branches or different cable properties along the cable length in an algorithmic fashion.

There are many types of beam elements available in the literatures for modeling cable systems (Schrefler and Odorizzi, 1983). The simplest one is the two-noded straight element. However, the straight element violates the continuity condition of slope and curvature of the slacking cable by discretizing the curved cable into straight segments and as a result excessive bending stiffness or membrane locking become prevalent (Cantin and Clough, 1968). Curved beam elements, which are based on the curvilinear strain field description, have an advantage over their straight counterparts in modeling curved cables with higher accuracy by coarse meshes. However, the formulation of curved beams is not a simple extension of the straight beam formulations because of the membrane locking problem. The earliest curved beam elements exhibited excessive bending stiffness when C^0-continuous axial and C^1-continuous transverse displacements are employed (Cantin and Clough, 1968). This phenomenon was initially attributed to the inability of low order polynomial interpolation to represent rigid body motion of the curved element properly (Ashwell and Sabir, 1971). The requirement for the terms of rigid body motion in interpolation function transfers the kinematic equations of membrane strain and curvature rate of curved beam into a second order homogeneous differential equation. The solutions of the differential equations, which are in terms of trigonometric functions, describe the rigid body modes of the curved beam. The addition of trigonometric terms to the polynomial displacement fields yielded better results (Ashwell and Sabir, 1971; Guimaraes and Heppler, 1997). Unfortunately, the trigonometric terms will provide a trivial solution, as the curvature of the beam approaches zero and the degenerated displacement fields are insufficient to represent the bending deformation of the straightened beam. However, studies (Dawe, 1976; Meck, 1980) show that adopting higher order polynomial displacement fields would alleviate the membrane locking. For instance, quintic polynomials have been used to interpolate the transverse and axial displacement fields of two-noded, planar curved beam element with

six degrees of freedom per node. It was further discovered by Meck (1980) that a more reliable curved beam element could be developed by using coupled high order polynomial displacement fields that recovered the inextensible bending mode of the curved beam. Later, Stolarski and Belytschko (1981) and Prathap and Bhashyam (1982) identified the cause of the locking as the failure of the independently interpolated displacement fields to recover correct constraints from the membrane strains in the state of inextensible bending and not because those displacement fields did not contain rigid body modes explicitly. Accordingly, reduced integration of membrane strain energy was proposed to improve the behavior of the curved beam element. Prathap and Bhashyam (1986) and Balasubramanian and Prathap (1989) further proposed a field consistency interpolation method, in which the axial displacement field is required to be one order higher than the transverse displacement field. The field consistency concept seems to be the most appealing among the curved beam element formulations, since it allows predicting a priori any poor convergence due to locking. Detailed reviews of curved element formulations can be found in the works of Raveendranath et al. (1999, 2000, 2001) and Bucalem and Bathe (1995). Although successful in eliminating membrane locking, it has been noticed that the relatively high accuracy of the above approaches is generally coupled with much more complicated mathematical formulations and cumbersome numerical computations. To reduce the computational burden, while being able to recover the inextensible bending mode of a curved beam, lower order polynomial displacement fields have been developed for curved beam elements by coupling the axial and transverse polynomial interpolations through the equilibrium equations (Raveendranath et al., 1999). To avoid the mathematical complexity of coupling through the equilibrium equations, Zhu and Meguid (accepted for publication) proposed a three-noded, three-dimensional curved beam element by coupling the consistent axial and transverse polynomial interpolations with presumably linear membrane and torsional strain fields. The new element demonstrates greater accuracy, faster convergence rate and better computational efficiency. However, the authors are unaware of any work that reports the application of curved beam elements in modeling low tension cable systems.

In this paper, we address and overcome these difficulties by developing a new nonlinear three-noded curved beam element that is capable of modeling the dynamics of low tension cable based on our previously proposed three-noded curved beam element (Zhu and Meguid, accepted for publication). The finite element formulation of the new curved beam element is developed by a variational approach using the principle of virtual work in the framework of incremental Updated Lagrange description. For the sake of the stability and the reliability of the numerical integration, the predictor–corrector method with Newmark (1959) time stepping algorithm and Newton–Raphson iteration is used to solve the equation of motion of low tension cables. The resulting finite element formulations and the time integration method are implemented in an appropriate computer program and validated by theoretical analyses and experimental investigations.

This paper contains five sections. Following this introductory section, Section 2 provides a detailed account of the newly developed curved beam element using updated Lagrangian formulations. In Section 3, we validate the newly developed curved beam element by various existing static and dynamic examples. In Section 4, we validate the newly developed curved beam element experimentally using a freely swinging steel cable and high speed imaging setup. The steel cable was strain gauged to allow the strain and load measurements. Finally, in Section 5, we conclude the paper.

2. Finite element formulation of three-noded curved beam element

Consider the three-noded curved beam element shown in Fig. 1. In order to describe the curved beam and its motion, a system of convected curvilinear coordinates, which are moved along with the beam material, is the most appropriate one, such as, x_i $(i = 1, 2, 3)$. The choice of coordinates is made in such a way that x_3 denotes the length along the neutral axis, and x_1 and x_2 denote the distances along lines orthogonal to the neutral axis. The incremental translational and rotational displacements of the neutral axis ${}_{t}u_1$, ${}_{t}u_2$,

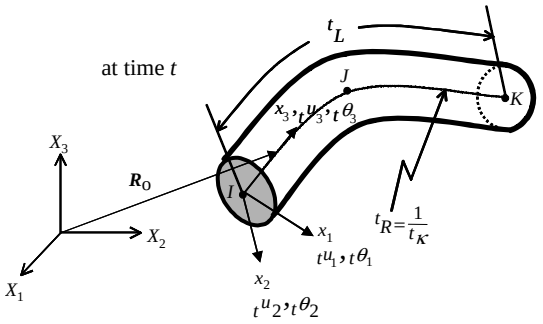

Fig. 1. Three-dimensional curved beam element in curvilinear coordinates.

${}_tu_3$, ${}_t\theta_1$, ${}_t\theta_2$, ${}_t\theta_3$ with respect to time t configuration are shown in the local curvilinear coordinate system in their respective positive directions. The geometry of the curved element will be described by its length ${}^tL$ and curvature ${}^t\kappa$ while the position and the orientation of the element in space will be determined by its nodal coordinates X_i $(i = 1, 2, 3)$ in a global Cartesian coordinate system. The transformation between the global and local coordinates will be established in accordance with Choi and Lim (1995).

The incremental Green–Lagrange strains of the curved beam at time $t + \Delta t$ are defined with respect to time t (Zhu, 2004), such as,

$$ {}_tE_{33} = {}_t\varepsilon - x_1({}_t\omega_2 - 2{}^t\kappa\,{}_t\varepsilon) + x_2\,{}_t\omega_1, \quad {}_tE_{13} = -\frac{x_2}{2}\,{}_t\eta, \quad {}_tE_{23} = \frac{x_1}{2}\,{}_t\eta \tag{1}$$

where ${}_t\varepsilon$, ${}_t\omega_1$, ${}_t\omega_2$, ${}_t\eta$ are the incremental membrane strain and curvature rates of the neutral axis and can be expressed in terms of the displacements of the neutral axis,

$$ {}_t\varepsilon = {}_tu_{3,3} - {}^t\kappa\,{}_tu_1 + \underline{\frac{1}{2}({}_tu_{1,3} + {}^t\kappa\,{}_tu_1)^2 + \frac{1}{2}({}_tu_{2,3})^2 + \frac{1}{2}({}_tu_{3,3} - {}^t\kappa\,{}_tu_1)^2} \tag{2a}$$

$$ {}_t\omega_1 = -{}_tu_{2,33} + {}^t\kappa\,{}_t\theta_3 \underline{+ {}_t\theta_3({}_tu_{1,33} + 2{}^t\kappa\,{}_tu_{3,3} - {}^t\kappa^2\,{}_tu_1) + {}_tu_{2,3}({}_tu_{3,33} - 2{}^t\kappa\,{}_tu_{1,3} - {}^t\kappa^2\,{}_tu_3)} \tag{2b}$$

$$ {}_t\omega_2 = {}_tu_{1,33} + {}^t\kappa\,{}_tu_{3,3} + {}^t\kappa\,{}_t\varepsilon^L \underline{+ {}_t\theta_3\,{}_tu_{2,33} - ({}_tu_{1,3} + {}^t\kappa\,{}_tu_3)({}_tu_{3,33} - 2{}^t\kappa\,{}_tu_{1,3} - {}^t\kappa^2\,{}_tu_3)} \tag{2c}$$

$$ {}_t\eta = {}_t\theta_{3,3} + {}^t\kappa\,{}_tu_{2,3} \underline{+ {}^t\kappa\,{}_t\theta_3({}_tu_{1,3} + {}^t\kappa\,{}_tu_3) + {}_tu_{2,3}({}_tu_{1,33} + {}^t\kappa\,{}_tu_{3,3})} \tag{2d}$$

The underlined terms in the above expressions are the nonlinear parts of the incremental membrane strain and curvature rates of the neutral axis due to the large displacements and rotations.

The incremental stress and strain of an elastic solid at time t obey the Hook's law, such that,

$$ {}_tS_{ij} = {}_tC_{ijkl}\,{}_tE_{kl} \tag{3}$$

where ${}_tC_{ijkl}$ is elastic constant tensor and ${}_tS_{ij}$ is the incremental second Piola–Kirchhoff stress tensor, respectively. By substituting Eqs. (1) and (2) into Eq. (3) and then calculating the stress resultant and couplings over the beam cross-section, we derive the incremental constitutive relationships of the curved beam as,

$$ {}_tT = \Delta T + \underline{{}_tu_{3,3}\,{}^{t+\Delta t}T + {}_t\theta_{1,3}\,{}^{t+\Delta t}M_1 + {}_t\theta_{2,3}\,{}^{t+\Delta t}M_2} \tag{4a}$$

$$ {}_tM_1 = \Delta M_1 + \underline{{}_tu_{3,3}\,{}^{t+\Delta t}M_1 + {}^{t+\Delta t}M_3\,{}_t\theta_2\,{}^tI_1/{}^tJ + {}^{t+\Delta t}T\,{}_t\theta_{1,3}\,{}^tI_1/{}^tA} \tag{4b}$$

$$ {}_tM_2 = \Delta M_2 + \underline{{}_tu_{3,3}\,{}^{t+\Delta t}M_2 - {}^{t+\Delta t}M_3\,{}_t\theta_1\,{}^tI_2/{}^tJ + {}^{t+\Delta t}T\,{}_t\theta_{2,3}\,{}^tI_2/{}^tA} \tag{4c}$$

$$ {}_tM_3 = \Delta M_3 - {}_tu_{1,3}\,{}^{t+\Delta t}M_1 - {}_tu_{2,3}\,{}^{t+\Delta t}M_2 + {}^{t+\Delta t}T\,{}_t\theta_{3,3}\,{}^tJ/{}^tA \tag{4d} $$

where ΔT and ΔM_i $(i=1,2,3)$ are the linear parts of the incremental tension, bending and torsional moments, the underlined terms are the nonlinear increments due to the large displacements and rotations, and ${}^tA$, ${}^tI_i$ $(i=1,2)$ and ${}^tJ$ are the area, principal and polar inertia moments of the cross-section of the beam, respectively.

The linear parts of the incremental tension, bending and torsional moments satisfy the following relationships, such that,

$$ \begin{Bmatrix} \Delta T \\ \Delta M_1 \\ \Delta M_2 \\ \Delta M_3 \end{Bmatrix} = \begin{bmatrix} {}_tE\,{}^tA & 0 & 0 & 0 \\ 0 & {}_tE\,{}^tI_1 & 0 & 0 \\ 0 & 0 & {}_tE\,{}^tI_2 & 0 \\ 0 & 0 & 0 & {}_tG\,{}^tJ \end{bmatrix} \begin{Bmatrix} {}_t\varepsilon \\ {}_t\omega_1 \\ {}_t\omega_2 \\ {}_t\eta \end{Bmatrix} \tag{4e} $$

where ${}_tE$ and ${}_tG$ are Young's and shear modulus, respectively.

As mentioned earlier, the fundamental condition for membrane locking-free element is that the displacement interpolation functions shall be able to recover the inextensible bending mode of a curved beam in which the membrane strain is zero (Stolarski and Belytschko, 1981; Prathap and Bhashyam, 1982). By ignoring the higher order terms in Eq. (2a), the fundamental condition can expressed approximately as,

$$ {}_t\varepsilon \approx {}_tu_{3,3} - {}^t\kappa\,{}_tu_1 = 0 \tag{5} $$

With this in mind, a simple and efficient approach is proposed herein to derive lower order coupled consistent polynomial interpolations for a curved beam element. First, assume that the interpolation functions for the transverse displacement fields (${}_tu_1$ and ${}_tu_2$) are quintic polynomials, which would represent the bending deformation of a three-noded curved beam element accurately, such that,

$$ {}_tu_1 = a_0 + a_1x_3 + a_2x_3^2 + a_3x_3^3 + a_4x_3^4 + a_5x_3^5 \tag{6a} $$

$$ {}_tu_2 = b_0 + b_1x_3 + b_2x_3^2 + b_3x_3^3 + b_4x_3^4 + b_5x_3^5 \tag{6b} $$

where a_i and b_i are the coefficients of the interpolation functions.

Then, the axial displacement ${}_tu_3$ is obtained by integrating the presumably linearly distributed membrane strain along the curved beam element, such that,

$$ {}_tu_3 = \int ({}_t\varepsilon + {}^t\kappa\,{}_tu_1)\,\mathrm{d}x_3 = a_6 + a_7x_3 + a_8x_3^2 + \frac{{}^t\kappa}{3}a_2x_3^3 + \frac{{}^t\kappa}{4}a_3x_3^4 + \frac{{}^t\kappa}{5}a_4x_3^5 + \frac{{}^t\kappa}{6}a_5x_3^6 \tag{7} $$

Substituting the displacements ${}_tu_1$ and ${}_tu_3$ into the inextensible bending condition Eq. (5) leads to

$$ {}_t\varepsilon \approx {}_tu_{3,3} - {}^t\kappa\,{}_tu_1 = a_7 - {}^t\kappa a_0 + (2a_8 - {}^t\kappa a_1)x_3 = 0 \tag{8} $$

Eq. (8) leads to the constraint equations of the inextensible bending mode, such that,

$$ a_7 - {}^t\kappa a_0 = 0 \quad 2a_8 - {}^t\kappa a_1 = 0 \tag{9} $$

Eq. (9) shows that there are no spurious terms in the constraint equations since each constraint equation contains the contributions from the axial and transverse displacement fields. Thus, the proposed displacement fields are able to recover the inextensible bending mode of the curved beam element, which ensures that the proposed interpolations are free from the membrane locking.

Secondly, it is noticed from the torsional strain expression that the torsional displacement ${}_t\theta_3$ is coupled with the transverse displacement ${}_tu_2$. Similar to the axial displacement interpolation, the interpolation for the torsional displacement is derived by assuming a linearly distributed torsional strain along the curved beam element, such that,

$$ {}_t\theta_3 = \int ({}_t\eta - {}^t\kappa\, {}_tu_{2,3})\,\mathrm{d}x_3 = b_6 + b_7x_3 + b_8x_3^2 - {}^t\kappa b_3x_3^3 - {}^t\kappa b_4x_3^4 - {}^t\kappa b_5x_3^5 \tag{10} $$

Finally, the complete set of interpolations for the three-noded curved beam element can be written as,

$$ {}_tu_1 = a_0 + a_1x_3 + a_2x_3^2 + a_3x_3^3 + a_4x_3^4 + a_5x_3^5 \tag{11a} $$

$$ {}_tu_2 = b_0 + b_1x_3 + b_2x_3^2 + b_3x_3^3 + b_4x_3^4 + b_5x_3^5 \tag{11b} $$

$$ {}_tu_3 = a_6 + a_7x_3 + a_8x_3^2 + \frac{{}^t\kappa}{3}a_2x_3^3 + \frac{{}^t\kappa}{4}a_3x_3^4 + \frac{{}^t\kappa}{5}a_4x_3^5 + \frac{{}^t\kappa}{6}a_5x_3^6 \tag{11c} $$

$$ {}_t\theta_1 = -b_1 - 2b_2x_3 - 3b_3x_3^2 - 4b_4x_3^3 - 5b_5x_3^4 \tag{11d} $$

$$ {}_t\theta_2 = (a_1 + {}^t\kappa a_6) + (2a_2 + {}^t\kappa a_7)x_3 + (3a_3 + {}^t\kappa a_8)x_3^2 + \left(4a_4 + \frac{{}^t\kappa^2}{3}a_2\right)x_3^3 + \left(5a_5 + \frac{{}^t\kappa^2}{4}a_3\right)x_3^4 + \frac{{}^t\kappa^2}{5}a_4x_3^5 + \frac{{}^t\kappa^2}{6}a_5x_3^6 \tag{11e} $$

$$ {}_t\theta_3 = b_6 + b_7x_3 + b_8x_3^2 - {}^t\kappa b_3x_3^3 - {}^t\kappa b_4x_3^4 - {}^t\kappa b_5x_3^5 \tag{11f} $$

It can be easily seen that the above displacement interpolations reduce to those of a three-noded straight beam element, if the curvature of the beam approaches zero. This indicates that the newly proposed curved beam element is applicable to both curved and straight beam analyses.

By using the incremental principle of virtual work at time $t + \Delta t$ with respect to the reference configuration at time t in the updated Lagrangian description, such as,

$$ \int_{{}_tV} {}^{t+\Delta t}S_{ij}\delta\, {}_tE_{ij}\,\mathrm{d}\,{}^tV - \int_{{}_tA_\sigma} {}^{t+\Delta t}p_i\delta\, {}_tu_i\,\mathrm{d}\,{}^tA - \int_{{}_tV} {}^{t+\Delta t}b_i\delta\, {}_tu_i\,\mathrm{d}\,{}^tV + \int_{{}_tV} {}^{t+\Delta t}\rho\, {}_t\ddot{u}_i\delta\, {}_tu_i\,\mathrm{d}\,{}^tV = 0 \tag{12} $$

we derive the discretized finite element equation of motion of the curved beam element,

$$ [{}_t^tM]\{{}_t\ddot{\boldsymbol{u}}\} + [{}_t^tC]\{{}_t\dot{\boldsymbol{u}}\} + [{}_t^tK]\{{}_t\boldsymbol{u}\} = \{{}^{t+\Delta t}\boldsymbol{F}\} - \{{}^t\boldsymbol{F}_S\} - \{{}^t\boldsymbol{F}_I\} \tag{13} $$

where $[{}_t^tM]$, $[{}_t^tC]$, $[{}_t^tK]$ are the mass, damping and stiffness matrixes, $\{{}_t\ddot{\boldsymbol{u}}\}$, $\{{}_t\dot{\boldsymbol{u}}\}$, $\{{}_t\boldsymbol{u}\}$ are the acceleration, velocity and displacement vectors, $\{{}^{t+\Delta t}\boldsymbol{F}\}$, $\{{}^t\boldsymbol{F}_S\}$, $\{{}^t\boldsymbol{F}_I\}$ are the external load, initial stress and inertia load vectors, respectively. The damping matrix in Eq. (13) is the Rayleigh damping (Rao, 1995) which is defined as,

$$ [{}_t^tC] = \alpha_v[{}_t^tM] + \beta_v[{}_t^tK] $$

$$ \alpha_v = \frac{4\pi f_1f_2(f_2\xi_1 - f_1\xi_2)}{f_2^2 - f_1^2}, \quad \beta_v = \frac{f_2\xi_2 - f_1\xi_1}{\pi(f_2^2 - f_1^2)} \tag{14} $$

where α_v and β_v are the Rayleigh damping coefficients, f_1 and f_2 are the lower and upper bound frequencies of interest in Hz, and ξ_1 and ξ_2 are the corresponding critical damping ratios, respectively.

The equation of motion (13) will be solved numerically by the predictor–corrector method using Newmark (1959) time stepping scheme with Newton–Raphson iteration (Hughes et al., 1979). The process of the predictor–corrector method may be outlined as follows,

(i) Predict displacement $\{{}^{t+\Delta t}\boldsymbol{u}^{(i)}\}$, velocity $\{{}^{t+\Delta t}\dot{\boldsymbol{u}}^{(i)}\}$, and acceleration $\{{}^{t+\Delta t}\ddot{\boldsymbol{u}}^{(i)}\}$ at time $t + \Delta t$ by

$$ \{{}^{t+\Delta t}\boldsymbol{u}^{(i)}\} = \{{}^{t+\Delta t}\tilde{\boldsymbol{u}}\} = \{{}^t\boldsymbol{u}\} + \{{}^t\dot{\boldsymbol{u}}\}\Delta t + \left(\frac{1}{2} - \beta\right)\Delta t^2\{{}^t\ddot{\boldsymbol{u}}\} \tag{15} $$

$$\{^{t+\Delta t}\dot{\boldsymbol{u}}^{(i)}\} = \{^{t+\Delta t}\tilde{\dot{\boldsymbol{u}}}\} = \{^{t}\dot{\boldsymbol{u}}\} + (1-\alpha)\Delta t\{^{t}\ddot{\boldsymbol{u}}\} \tag{16}$$

$$\{^{t+\Delta t}\ddot{\boldsymbol{u}}^{(i)}\} = \{^{t+\Delta t}\tilde{\ddot{\boldsymbol{u}}}\} = \frac{\{^{t+\Delta t}\boldsymbol{u}^{(i)}\} - \{^{t+\Delta t}\tilde{\boldsymbol{u}}\}}{\beta\Delta t^2} = 0 \tag{17}$$

(ii) Form effective stiffness matrix $[{}_t{}^t\boldsymbol{K}_e]$ and calculate residual force $\{\boldsymbol{R}({}_t\boldsymbol{u}^{(i)})\}$

$$[{}_t{}^t\boldsymbol{K}_e] = \frac{1}{\beta\Delta t^2}[{}_t{}^t\boldsymbol{M}] + \frac{\alpha}{\beta\Delta t}[{}_t{}^t\boldsymbol{C}] + [{}_t{}^t\boldsymbol{K}] \tag{18}$$

$$\{\boldsymbol{R}({}_t\boldsymbol{u}^{(i)})\} = [{}_t{}^t\boldsymbol{K}_e]\{{}_t\boldsymbol{u}^{(i)}\} = \{^{t+\Delta t}\boldsymbol{F}\} - \{^{t+\Delta t}\boldsymbol{F}_I^{(i)}\} - \{^{t+\Delta t}\boldsymbol{F}_S^{(i)}\} \tag{19}$$

(iii) Solve for correction $\{{}_t\boldsymbol{u}^{(i)}\}$ and correct previous solutions

$$\{^{t+\Delta t}\boldsymbol{u}^{(i+1)}\} = \{^{t+\Delta t}\boldsymbol{u}^{(i)}\} + \{{}_t\boldsymbol{u}^{(i)}\} \tag{20}$$

$$\{^{t+\Delta t}\ddot{\boldsymbol{u}}^{(i+1)}\} = \frac{\{^{t+\Delta t}\boldsymbol{u}^{(i+1)}\} - \{^{t+\Delta t}\tilde{\boldsymbol{u}}\}}{\beta\Delta t^2} \tag{21}$$

$$\{^{t+\Delta t}\dot{\boldsymbol{u}}^{(i)}\} = \{^{t+\Delta t}\tilde{\dot{\boldsymbol{u}}}\} + \Delta t\{^{t+\Delta t}\ddot{\boldsymbol{u}}^{(i+1)}\} \tag{22}$$

If the residual force or the correction to the displacement is greater than the prescribed tolerance and additional iterations are to be performed, i is replaced by $i+1$, and calculations resume with (18). In the above equations, the α and β are the Newmark's time integration parameters and can be determined by

$$\alpha = \frac{3-\rho_\infty}{2(1+\rho_\infty)}, \quad \beta = \frac{1}{(1+\rho_\infty)^2} \tag{23}$$

where ρ_∞ is a spectral radius representing the numerical damping in the high frequency limit (usually user-defined high frequency dissipation). This numerical dissipation varies from no dissipation case, $\rho_\infty = 1$, to so-called asymptotic annihilation case, $\rho_\infty = 0$.

3. Numerical verification of curved beam element

3.1. In-plane bending of one-half circular cantilever beam

Consider one-half of a circular cantilever beam fixed at one end and subjected to a load at its free end as shown in Fig. 2. The theoretical solutions of the tip displacements are obtained using Castigliano's energy theorem:

$$u = \frac{2PR^3}{EI}, \quad v = \frac{3\pi}{2}\frac{PR^3}{EI} + \frac{\pi}{2}\frac{PR}{EA}, \quad \theta_z = \frac{\pi PR^2}{EI} \tag{24}$$

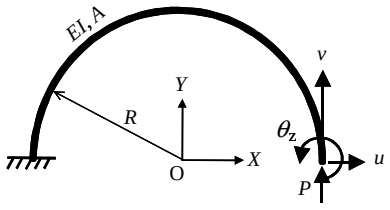

Fig. 2. Cantilevered one-half circular beam with in-plane tip load.

By using only one newly developed curved beam element, we derive the tip displacements as,

$$u_f \approx 1.00072\frac{2PR^3}{EI}, \quad v_f \approx 0.99980\frac{3\pi PR^3}{2EI} + 0.98578\frac{\pi PR}{2EA}, \quad \theta_{zf} \approx 0.99997\frac{\pi PR^2}{EI} \tag{25}$$

Considering the fact $\frac{PR^3}{EI} / \frac{PR}{EA} \gg 1$ for slender beams, Eq. (25) indicates that the idealization with only one newly developed three-noded curved element efficiently converges to the theoretical solution with discrepancies less than 0.02%.

3.2. Three-dimensional deformation of helical spring

A three-dimensional curved structure such as the one turn of a helical spring and its material and geometric properties are shown in Fig. 3. The spring is fixed at one end and is subjected a concentrated load at the other end. The theoretical deflection of the spring at loading point can be obtained from Castigliano's energy theorem

$$v = \frac{\pi PR^3}{\cos\alpha EI_{xx}} + \frac{3\pi PR^3}{\cos\alpha GJ} \tag{26}$$

The spring was modeled with the newly developed three-noded curved beam element and the finite element solutions are normalized by the theoretical solution of Eq. (26). Fig. 4 shows the comparisons of the finite element solutions of new and existing beam elements vs. the number of element. It can be seen that a quite accurate result can be obtained by using only two newly developed three-noded curved beam elements with a discrepancy of less than 0.4%. By using four new curved beam elements, the finite element solution is almost the same as the theoretical solution. The results of a straight element and a comparable three-noded curved element by Choi and Lim (1995) are also depicted for comparison. The straight element exhibits strong membrane locking characteristics and consequently a fine mesh is required to ensure its convergence to the theoretical solution. The existing curved element converged to 98% of the theoretical solution by using eight elements. Obviously, the new curved beam element converges much faster than the existing earlier curved beam element considered in the comparison.

3.3. Large rotation of in-plane bending of cantilever beam

Consider an initially straight cantilever beam which is subjected to a concentrated moment M at its free end as shown in Fig. 5. The analytical solution (Shafr, 1999) shows that the deformed beam will be part of a circle of curvature of $\kappa = M/EI$, and the displacements of free end are

$$u = \frac{EI}{M}\sin\left(\frac{ML}{EI}\right) - L, \quad v = \frac{EI}{M}\left[1 - \cos\left(\frac{ML}{EI}\right)\right] \tag{27}$$

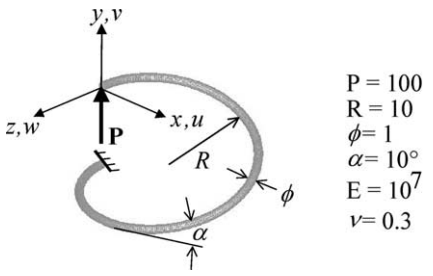

Fig. 3. A helical spring with point load at tip.

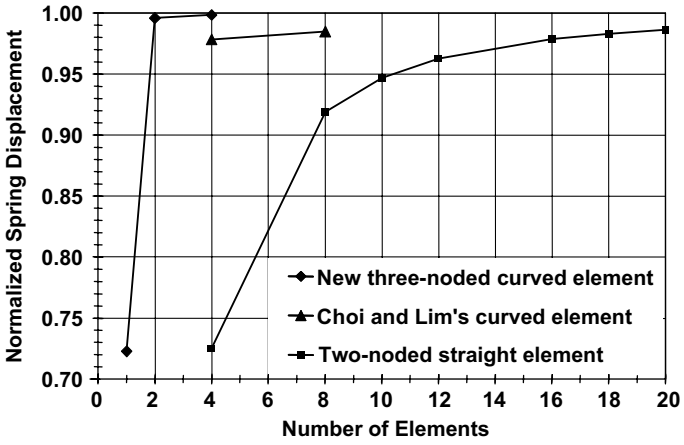

Fig. 4. Convergence of deflection at loading point of a helical spring.

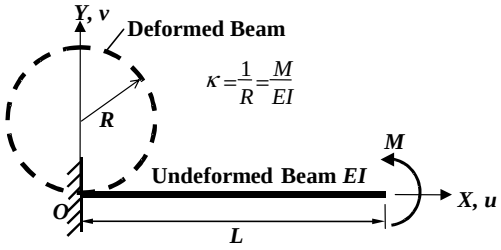

Fig. 5. Cantilever beam subjected to bending moment at its free end.

where EI and L are the rigidity and length of the beam, and κ is the curvature of the deformed beam, respectively. The same problem has been studied by Surana (1983), Lo (1992), and many other researchers with eight or more two-noded straight beam elements. In the present study, only two newly developed three-noded curved beam elements (15 DOF) are used to model the cantilever beam. The dimensionless results of present analysis are shown in Fig. 6 to demonstrate how the newly derived curved beam element performs numerically. Note that the load factor is $\lambda = LM/\pi EI$. With only two new elements, the present results agree with the theoretical solutions even in the range of very large displacement and rotation, where the beam is bent into a circle by using 60 equal load increments. Compared with the results of Lo (1992), which employed eight straight beam elements (27 DOF), it has been shown that the present results agree with the theoretical solutions better in very large displacement and rotation situation.

3.4. Natural frequencies of U-bend beam

The U-bend beam with intermediate supports is shown in Fig. 7. The rotational inertia has been neglected, except the rotary inertia associated with the beam twisting about its own axis. The half circular portion is modeled by six newly developed three-noded curved beam elements and the two straight legs are modeled by one to four new elements depending on the length of these legs. The natural frequencies of first two modes of in-plane and out-of-plane vibrations of the U-bend are shown in Fig. 8. The results of the newly developed curved beam element agree with the Blevins' (1979) numerical results very well.

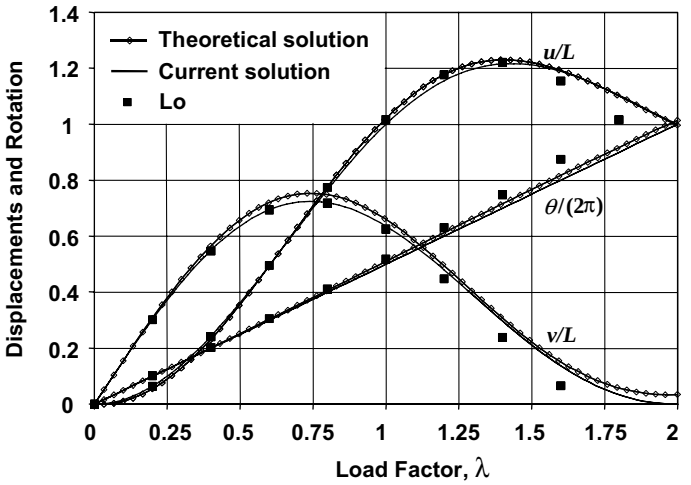

Fig. 6. Comparison of tip displacements and rotation of cantilever beam.

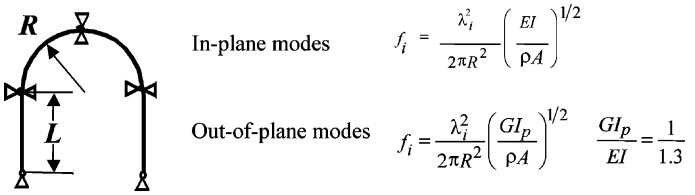

Fig. 7. Free vibration of U-bend beam with intermediate supports.

4. Experimental investigation

The setup of the free swing experiment of an instrumented cable is shown schematically in Fig. 9. The cable is initially simply supported at both ends by circular pins and then released from the temporary support to allow it swing freely. A high speed digital camera records the motion of the swinging cable while an oscilloscope records the time history of cable tension at simply supported end by strain gauges. The selected test piece is a 6.5 mm diameter, 6×7 with 1×7 WSC steel cable of 1668 mm long. Its effective area and moment inertia of cross-section are 19.62 mm^2 and 2.71 mm^4, respectively. The cable density is 0.15 kg/m and its elastic modulus is 53 GPa. There are two aluminum blocks attached to two ends as harnesses. The dimensions of the free end block are 100 mm × 50 mm × 25 mm while the block at the simply supported end is $45 \times 16 \times 6$ mm. Four 3.175 mm unidirectional strain gauges were mounted on two opposite faces of the block at the simply supported end in T-configurations to eliminate possible out-of-plane bending effects as well as to increase the gain of the strain gauge readings.

For the motion of low tension cable, the drag effect of the free end block becomes noticeable and could be determined as follows:

$$F = -1.1\rho_a D V^2 \tag{28}$$

where D is the characteristic transverse dimension of the block, ρ_a is the air density, V is the velocity of block, respectively.

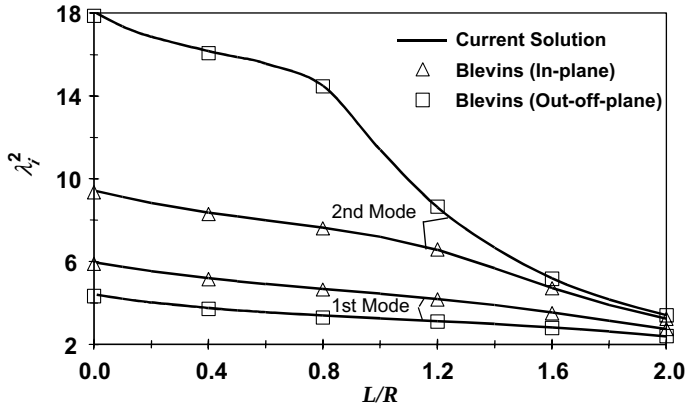

Fig. 8. Natural frequencies of U-bend beam vs. leg length.

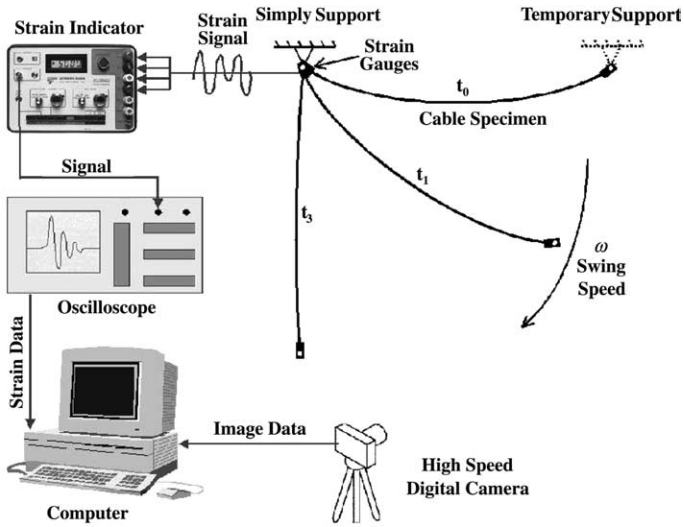

Fig. 9. Schematic of free swing cable experiment setup.

The experiments have been done with and without a lumped mass of 0.34 kg attached to the free end of the cable. The motion of the swinging cable was captured using the high speed digital camera at every 1/60 s and the cable tension was measured at the simply supported end by strain gauges at a sampling rate of 1000 Hz. The experiments show that the cable with the lumped mass is stable and swings in a pendulum mode, while the cable without the lumped mass slacks in the first two swings and then approaches the stable pendulum mode. Fig. 10(a) shows the successive positions of the first two swings of the cable without the lumped mass retracted from the motion images. It is noted that the cable whips in the first swing as it swings upwards to the highest position, and then slacks in the second swing as it falls from the highest position. Figs. 11 and 12 show the measured time histories of the position and the velocity of the free end of cable with lumped mass. Fig. 13 depicts the measurements of cable tension at the simply supported end vs. time.

The finite element analysis of the cable is carried out using 12 newly developed curved beam elements (10 for the cable and 2 for the end blocks) and one mass element for the lumped mass. The parameters for time

integration, such as the time step, the spectral radius of numerical damping and Rayleigh damping coefficients, were chosen carefully by examining the dynamic characteristics of the swinging cable. The experimental data of Fig. 11 shows that the frequency of the pendulum motion of the cable is 0.35 Hz and the logarithmic decrement is 0.02, which is equivalent to a critical damping ratio of 0.003 (Rao, 1995). In addition, the membrane natural frequency of the cable is 156 Hz, and its inherent damping is exceptionally low; usually less than 0.2% of critical damping, (Carrie, 1980). By substituting the above frequency and damping ratios into Eq. (14), we obtain the Rayleigh damping coefficients to be $\alpha_v \approx 10^{-2}$ and $\beta_v \approx 10^{-5}$. In addition, the work of an elastic pendulum by Kuhl and Crisfield (1999) demonstrated that the Newmark integration scheme with $\rho_\infty = 1.0$ is unstable in this class of nonlinear problem. A lower value of the spectral radius $\rho_\infty < 1.0$ is required to maintain the numerical stability. However, this selection would result in a decrease of total energy of the system. Consequently, a spectral radius of numerical damping of $\rho_\infty = 0.9$ was selected to provide the minimum required numerical damping to dissipate the spurious high frequency components, while minimizing the loss of the total energy. Finally, the finite element discretization of the cable results in a smallest modal period of 0.0004 s. A stable time step needs to be about one-tenth of the smallest period (Bathe, 1982). Thus, the time integration step was set to 5×10^{-5} s for our finite element analysis.

The positions of the cable without the lump mass predicted by finite element analysis are depicted in Fig. 10(b) together with the experimental measurements. It is shown that the finite element predictions and experimental measurements are in good agreement. Next, the predicted time histories of the position and the velocity of the free end of cable with lumped mass are shown in Figs. 11 and 12 against the experimental findings. It can be seen that the finite element results agree with the experimental data very well. Finally, the predicted time history of the cable tension with lumped mass at the simply supported end is shown in Fig. 13 against the experimental results. The finite element predictions and experimental results are in good agreement.

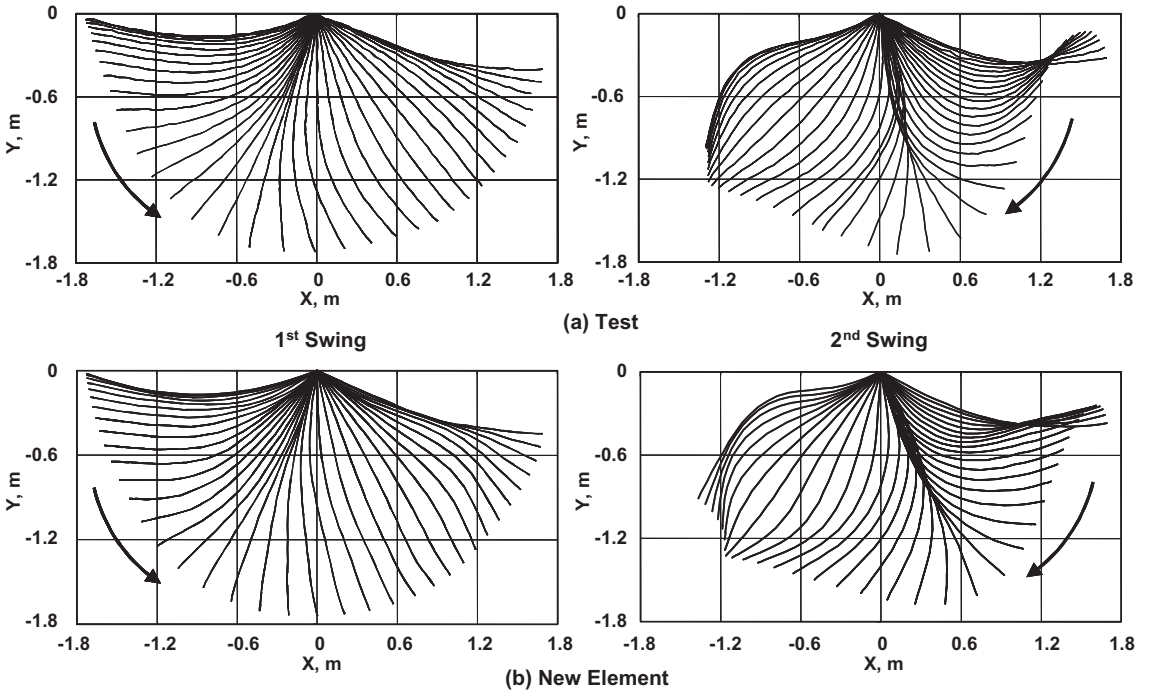

Fig. 10. Comparisons of positions of swinging cable without lumped mass: (a) test results and (b) FE predictions.

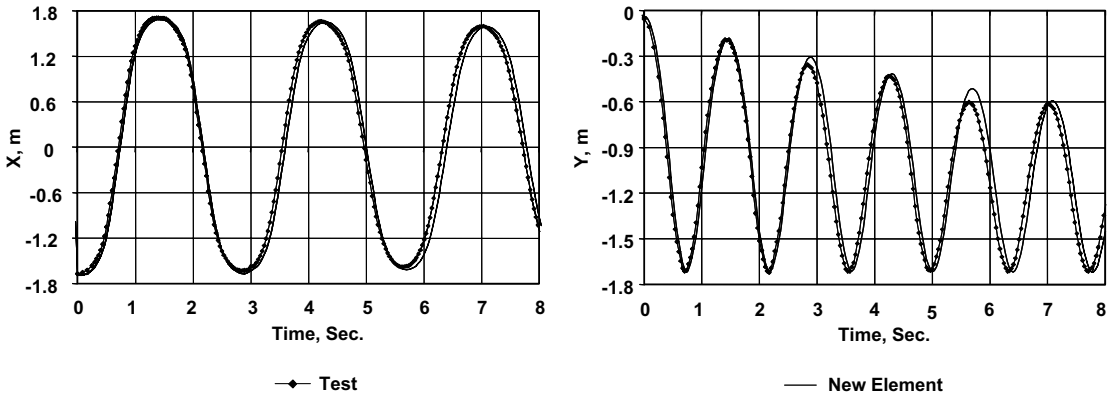

Fig. 11. Test results and FE predictions of position of free end of swinging cable with lumped mass.

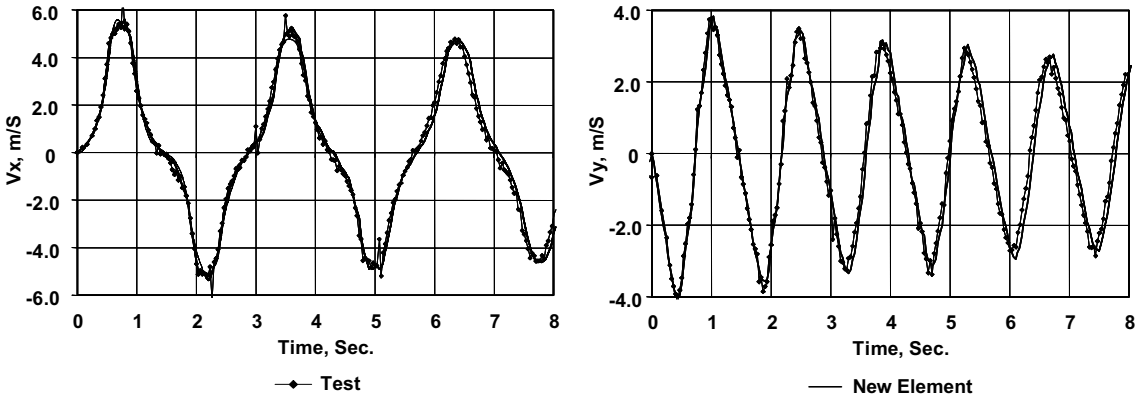

Fig. 12. Test results and FE predictions of velocity of free end of swinging cable with lumped mass.

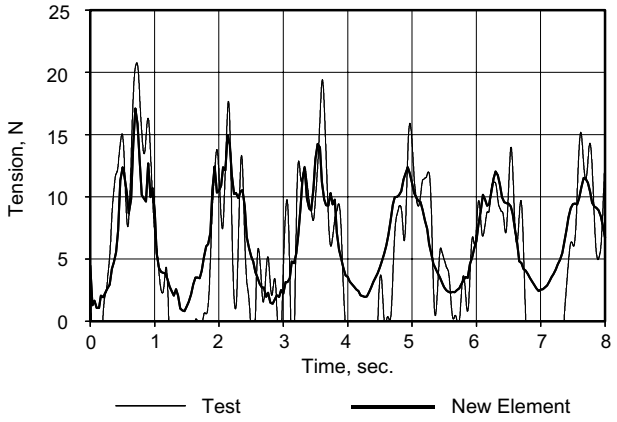

Fig. 13. Comparison of cable tension at simply supported end of swing cable with lumped mass.

5. Conclusion

Existing analyses of low tension cable systems are mostly restricted to the classic cable theory, in which the cable is idealized as a tensile member only. Under dynamic loading conditions, the slacking of the cable could result in zero cable tension and lead to singularity. In this paper, we address and overcome the difficulties associated with the singularity in the classic cable theory by developing an accurate and computationally efficient three-noded, curved beam element for the three-dimensional analysis of large displacements and rotations of curved beams. Consistently coupled polynomial interpolations are used to eliminate the membrane locking and ensure a faster convergence rate. Numerical results of two- and three-dimensional applications are presented to demonstrate the superior accuracy and the high convergence rate of the newly developed curved beam element compared with the existing ones. A predictor–corrector method is presented for the efficient and the reliable analysis of nonlinear dynamic behavior of low tension cables. Experiments involving the free swinging of a steel cable were conducted to validate the newly developed curved beam element and the predictor–corrector time integration algorithm. The experimental results are compared with the finite element predictions using the newly developed curved beam element. Very good agreements in position, velocity and tension of the cable are observed.

References

Ashwell, D.G., Sabir, A.B., 1971. Limitations of certain curved finite elements when applied to arches. International Journal of Mechanical Science 13, 133–139.

Balasubramanian, T.S., Prathap, G., 1989. A field consistent higher-order curved beam element for static and dynamic analysis of stepped arches. Computers and Structures 33, 281–288.

Bathe, K.J., 1982. Finite Element Procedures in Engineering Analysis. Prentice-Hall, Englewood Cliffs, New Jersey.

Blevins, R.D., 1979. Formulas for Natural Frequency and Mode Shape. Van Nostrand Reinhold Company, New York.

Bucalem, M.L., Bathe, K.J., 1995. Locking behavior of isoparametric curved beam finite elements. Applied Mechanics Review 48, S25–S29.

Buckham, B., Nahon, M., 1999. Dynamics simulation of low tension tethers. In: Proceedings of the OCEANS'99 MTS/IEEE, Seattle, USA, pp. 757–766.

Burgess, J.J., 1992. Equations of motion of a submerged cable with bending stiffness. Offshore Marine and Arctic Engineering 1-A, 283–289.

Cantin, G., Clough, R., 1968. A curved cylindrical shell finite element. AIAA 6, 1057–1062.

Carrie, T.G., 1980, Guy cable design and damping for vertical axis wind turbines. SAND80-2669, National Technical Information Service, US Department of Commerce.

Choi, J., Lim, J., 1995. General curved beam elements based on the assumed strain fields. Computers and Structures 55, 379–386.

Dawe, D.J., 1976. Some high-order elements for arches and shells. In: Ashwell, D.G., Gallagher, R.H. (Eds.), Finite Elements for Thin Shells and Curved Members. John Wiley, London, pp. 131–153.

Delmer, T.N., Stephens, T.C., Tremills, J.A., 1988. Numerical simulation of cable-towed acoustic arrays. Ocean Engineering 15 (6), 511–548.

Guimaraes, J.E.F., Heppler, G.R., 1997. On trigonometric basis functions for C1 curved beam finite elements. Computers and Structures 45, 405–413.

Howell, C.T., 1992. Numerical analysis of 2-D nonlinear cable equations with applications to low-tension problems. International Journal of Offshore and Polar Engineering 2 (2), 110–113.

Hughes, T.J.R., Pister, K.S., Taylor, R.L., 1979. Implicit-explicit finite elements in nonlinear transient analysis. Computer Methods in Applied Mechanics and Engineering 17/18, 159–182.

Koh, C.G., Zhang, Y., Quek, S.T., 1999. Low-tension cable dynamics: numerical and experimental studies. Journal of Engineering Mechanics 125 (3), 347–354.

Kuhl, D., Crisfield, M.A., 1999. Energy-conserving and decaying algorithms in non-linear structural dynamics. International Journal for Numerical Methods in Engineering 45, 569–599.

Leonard, J.W., Recker, W.W., 1972. Nonlinear dynamics of cables with low initial tension. Journal of Engineering Mechanics, ACSE 98, 293–309.

Lo, S.H., 1992. Geometrically nonlinear formulation of 3D finite strain beam element with large rotations. Computers and Structures 44, 147–157.

Meck, H.R., 1980. An accurate polynomial displacement function for finite elements. Computers and Structures 11, 265–269.
Newmark, N.M., 1959. A method of computation for structural dynamics. ASCE Journal of Engineering Mechanics Division 8, 67–94.
Phillips, W.H., 1949. Theoretical analysis of oscillations of a towed cable. NACA Technical Note No.1796.
Prathap, G., Bhashyam, G.R., 1982. Reduced integration and the shear flexible beam element. International Journal for Numerical Methods in Engineering 18, 195–210.
Prathap, G., Bhashyam, G.R., 1986. A linear thick curved beam element. International Journal for Numerical Methods in Engineering 23, 1313–1328.
Raveendranath, P., Singh, G., Pradhan, B., 1999. A two-noded locking-free shear flexible curved beam element. International Journal for Numerical Methods in Engineering 44, 265–280.
Raveendranath, P., Singh, G., Pradhan, B., 2000. Free vibration of arches using a curved beam element based on a coupled polynomial displacement field. Computers and Structures 78, 583–590.
Raveendranath, P., Singh, G., Rao, G.V., 2001. A three-noded shear-flexible curved beam element based on coupled displacement field interpolations. International Journal for Numerical Methods in Engineering 51, 85–101.
Rizzo, A.R., 1991. FE analysis simulates undersea structures. Mechanical Engineering, 51–54.
Rao, S.S., 1995. Mechanical Vibrations, third ed. Addison-Wesley Publishing Company Inc.
Schrefler, B.A., Odorizzi, S., 1983. A total lagrangian geometrically nonlinear analysis of combined beam and cable structures. Computer and Structures 17 (1), 115–127.
Shafr, I., 1999. Nonlinear strain measures, shape functions and beam elements for dynamics of flexible beams. Multibody System Dynamics 3, 189–205.
Stolarski, H., Belytschko, T., 1981. Membrane locking and reduced integration for curved elements. Journal of Applied Mechanics 49, 172–178.
Sun, Y., Leonard, J.W., 1998. Hybrid cable/elastica model for low tension cable deployment problemsProceedings of the International Offshore and Polar Engineering Conference, vol. 2. ISOPE, Golden, USA, pp. 233–238.
Surana, K.S., 1983. Geometrically nonlinear formulation for the curved shell elements. International Journal of Numerical Methods in Engineering 19, 581–615.
Vassberg, J.C., Yeh, D.T., Blair, A.J., Evert, J.M., 2002. Dynamic characteristics of a KC-10 wing-pod refueling hose by numerical simulation. In: 20th AIAA Applied Aerodynamics Conference, Paper No. AIAA 2002-2712, St. Louis, Missouri, USA.
Vassalos, D., Huang, S., 1996. Dynamics of small-sagged taut-slack marine cables. Computers and Structures 58 (3), 557–562.
Wu, Q., Takahashi, K., Nakamura, S., 2003. Non-linear vibrations of cables considering loosening. Journal of Sound and Vibration 261, 385–402.
Zhu, Z.H., 2004. Nonlinear elastodynamic analysis of low tension cable using a new beam element. Ph.D. Thesis, University of Toronto, Toronto, Ontario, Canada.
Zhu, Z.H., Meguid, S.A., Ong, L.S., 2001. Dynamic multiscale simulation of towed cable and body. In: K.J. Bathe (Ed.), Proceedings of the Second MIT conference on Computational Fluid and Solid Mechanics. Paper No. 521.
Zhu, Z.H., Meguid, S.A., 2004. Analysis of three-dimensional locking-free curved beam element. International Journal of Computational Engineering Science, accepted for publication.